Journal of Physics A: Mathematical and Theoretical

TOPICAL REVIEW • **OPEN ACCESS**

The flow beneath a periodic travelling surface water wave

To cite this article: Adrian Constantin 2015 *J. Phys. A: Math. Theor.* **48** 143001

OPEN ACCESS
IOP Publishing
Journal of Physics A: Mathematical and Theoretical
J. Phys. A: Math. Theor. **48** (2015) 143001 (25pp)
doi:10.1088/1751-8113/48/14/143001

Topical Review

The flow beneath a periodic travelling surface water wave

Adrian Constantin

Department of Mathematics, King's College London, Strand, WC2R 2LS, UK
Faculty of Mathematics, University of Vienna, Oskar-Morgenstern-Platz 1, A-1090 Vienna, Austria

E-mail: adrian.constantin@kcl.ac.uk

Received 5 November 2014, revised 19 January 2015
Accepted for publication 23 January 2015
Published 20 March 2015

Abstract

We discuss some recent results on the behaviour of the velocity field, pressure and particle trajectories beneath a periodic travelling wave propagating at the surface of water with a flat bed, in a flow without underlying currents. By analysing the governing equations we avoid approximations, thus ensuring the validity of the results without restrictions on the wave amplitude. In particular, the presented approach applies to waves of large amplitude. We also formulate some open problems, venturing into the relatively unexplored field of wave–current interactions.

Keywords: water waves, hydrodynamics, vorticity

1. Introduction

The most regular water waves are the periodic travelling waves, propagating over long distances at practically constant speed, in a fixed direction, at the surface of water with a flat bed. The study of the flow beneath these waves, in the absence of non-uniform underlying currents, was initiated in the 19th century and represents a classical subject in hydrodynamics. For waves of very small amplitude, reliance on first-order approximations (linear theory) predicts closed particle paths, either circular (in deep water) or elliptical (in shallow water). This type of conclusion is presented in all standard textbooks on water waves [22, 24, 34, 41, 48, 57, 58]. However, as was pointed out by Stokes in a classical memoir (1847)—see [59]—the fact that all individual particles in an irrotational periodic travelling

wave propagating over an infinitely deep body of fluid describe exactly closed paths is prevented by the presence in the flow of a second-order mean velocity, called the 'mass-transport velocity' or 'Stokes drift'—see [27, 42]—in the direction of wave propagation. Ursell [64] investigated the corresponding phenomenon in water of finite depth, establishing also in this setting the existence of a second-order mean drift in the direction of wave propagation. The Stokes drift was analysed experimentally by Longuet-Higgins [43, 45], who concluded that in steep waves the closed orbits predicted by linear theory become quite distorted, the salient feature being a strong forward drift near the surface; for example, in a complete orbit a particle may advance horizontally through a distance 0.38 times the wavelength. These considerations show the importance of going beyond linear theory by accounting for nonlinear effects. Moreover, the fact that the Stokes drift is a mean velocity raises the issue of whether there is a regular pattern for the particle trajectories; or is the individual behaviour rather chaotic and all we can hope for is a statistical understanding of the motion, after averaging? An approach relying on perturbation theory presents insurmontable difficulties for steep waves owing to the unavailability of exact solutions other than uniform flows with a flat surface. Suitable approximations for steep waves exist only for the wave of maximum steepness (the Stokes wave of greatest height), which presents special features, e.g. a sharp-angled crest of 120°, so that its profile between two successive crests may be approximated by the arc of a circle [45]. This simple but accurate approximation permitted Longuet-Higgins [45] to describe the particle trajectories in this limiting case as loops with a depth-dependent forward drift that is maximal at the surface. Unfortunately, the special features of this limiting wave pattern do not persist for non-extreme steep waves, so that the unavailability of suitable approximations for steep waves has not been overcome. However, recent theoretical breaktroughs permit in-depth studies that uncover certain essential qualitative features of the flow beneath a steep wave. In particular, one can conclude that, in the absence of an underlying current, each particle path is a loop with a forward drift [9]. The deviation from a closed path is quite small for certain choices of mean depth, wavelength and wave height, as confirmed by recent accurate high-tech measurements [5, 63]. This explains why less accurate experiments performed some decades ago (with photographs reproduced in [24, 57, 58]) seem to indicate closed paths. The theoretical results on the particle trajectories are contingent on an interplay between properties of the velocity field and the pressure.

A further novel aspect regards the understanding of the behaviour of the pressure within the bulk of the fluid [17]. This led to some new approaches towards the recovery of the shape of the free surface wave from pressure measurements at the bed [8, 13, 38, 51]. Earlier attempts in this direction were performed within the framework of linear theory and presented large errors. Despite these achievements, there are a number of basic questions that are still open, for example concerning the monotonicity of the vertical velocity component [7]. Numerical simulations [49] and experimental data indicate a pattern that is yet to be confirmed theoretically so that its validity could be granted for all relevant physical regimes.

Our aim is to present the state-of-the-art for irrotational flows with no underlying curents, explaining the available results and formulating some current open problems. We will also venture into the uncharted territory of wave–current interactions, in which case the presence of non-zero vorticity gives rise to much more complex phenomena. A brief survey of some promising recent results will be presented and a selection from the extensive collection of open problems will be formulated.

2. The flow beneath a periodic travelling wave with no underlying current

Steadily-progressing periodic wave trains represent the simplest non-trivial water-wave pattern, and yet their study is difficult for a variety of reasons. The governing equations are nonlinear and represent a free-boundary problem: the location of the water's free surface is not known beforehand but must be determined as part of the solution.

Let us specify the simplifying assumptions that are commonly made to describe these waves. The wave dynamics is dominated by the inertia of the fluid, the pressure gradient, and gravitational acceleration. For large scale waves fluid viscosity can be neglected since it is important only in very thin layers near the boundaries. Also, the effects of surface tension are relevant only for waves of small amplitude. The absence of underlying currents is captured by assuming that the flow is irrotational, setting that is appropriate for waves propagating into a region of water previously at rest. Moreover, since the density of water is about 10^3 times that of air, we can neglect the airflow about the water. Finally, we consider the flow to be two-dimensional, that is, with no variations in a direction parallel to the crest, with the periodic wave profile propagating at constant speed in a fixed direction, at the surface of a layer of water with a horizontal flat bed. These wave patterns, having a clearly defined shape, speed and direction, are not generated by the local wind but by distant weather systems. They are termed *swell* or *Stokes waves*. To describe them it suffices to consider a cross section of the flow in the direction of wave propagation, by choosing Cartesian coordinates (X, Y) with the X-axis pointing in the direction of wave propagation and the Y-axis pointing vertically upwards, while the origin is located on the mean water level $Y = 0$ and the flat bed is given by $Y = -d$, where $d > 0$ is the mean depth. Let $(U(X, Y, T), V(X, Y, T)$ be the velocity field and let $Y = H(X, T)$ be the water's free surface, where T stands for time. For water of constant density the equation of mass conservation is

$$U_X + V_Y = 0 \tag{1}$$

throughout the fluid; see [10]. The equation of motion is Euler's equation

$$\begin{cases} U_T + UU_X + VU_Y = -\dfrac{1}{\rho}\mathcal{P}_X, \\ V_T + UV_X + VV_Y = -\dfrac{1}{\rho}\mathcal{P}_Y - g, \end{cases} \tag{2}$$

see [10], where $\mathcal{P}(X, Y, T)$ is the pressure, g is the (constant) acceleration of gravity and ρ is the constant density. We draw attention to the fact that while in a compressible fluid the pressure determines the density, the present incompressible context withholds this effect and $\mathcal{P}$ has to be regarded as a reaction to the constraint of incompressibility. The boundary conditions associated to (1) and (2) are

$$V = 0 \quad \text{on the flat bed} \quad Y = -d, \tag{3}$$

and

$$V = H_T + UH_X \quad \text{on} \quad Y = H(X, T), \tag{4}$$

as well as

$$\mathcal{P} = \mathcal{P}_{\text{atm}} \quad \text{on} \quad Y = H(X, T), \tag{5}$$

on the free surface. The kinematic boundary conditions (3) and (4) reflect the fact that both boundaries are interfaces: particles on these boundaries are confined to them at all times (see the discussion in [10]). The dynamic boundary condition (5), in which $\mathcal{P}_{\text{atm}}$ stands for the

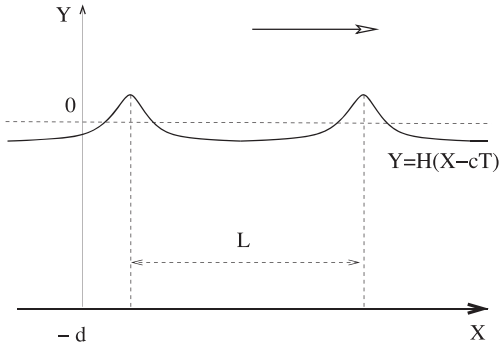

Figure 1. The Stokes wave in physical coordinates. Typical features of the wave profile are the sharp crests and flat troughs. This crest/trough asymmetry is in contrast to the sinusoidal waves $Y = \varepsilon \cos\left(\frac{2\pi(X-cT)}{L}\right)$ encountered in linear water-wave theory. See [10] for some striking photographs of Stokes waves.

(constant) atmospheric pressure at the surface, decouples the motion of the water from that of the air above. The condition of irrotational flow is expressed by

$$U_Y = V_X \tag{6}$$

throughout the fluid, while the setting of travelling waves corresponds to an (X, T)-dependence of the free surface H, of the pressure $\mathcal{P}$ and of the velocity field (U, V) in the form $(X - cT)$, where $c > 0$ is the (constant) propagation speed. Periodicity means an L-periodic X-dependence of all these unknown functions, where $L > 0$ represents the wavelength; see figure 1. The equations (1)–(6) are the governing equations for irrotational travelling gravity water waves. Their nonlinear character is clearly visible in (2) and (4), being also hidden in (5), cf the discussion in section 2.1.1. As already pointed out, we deal with a free-boundary problem, since H is unknown. Another important aspect concerns the fact that (6) only guarantees that an underlying current must be uniform, and the absence of an underlying current amounts to imposing the condition of a vanishing mean flow; see (20) below. The considerations in section 2.1.1 will also clarify the non-trivial issue of the definition of the wave speed c.

2.1. Re-formulations of the governing equations

We can remove time from the governing equations by introducing the moving frame

$$x = X - cT, \qquad y = Y. \tag{7}$$

Setting

$$u(x, y) = U(X - cT, Y), \quad v(x, y) = V(X - cT, Y),$$
$$\eta(x) = H(X - cT), \quad P(x, y) = \frac{1}{\rho}\mathcal{P}(X - cT, Y), \tag{8}$$

in the moving frame the equation of mass conservation (1) becomes

$$u_x + v_y = 0, \tag{9}$$

Euler's equation (2) takes on the form

$$\begin{cases} (u-c)u_x + vu_y = -P_x, \\ (u-c)v_x + vv_y = -P_y - g, \end{cases} \tag{10}$$

while

$$u_y = v_x \tag{11}$$

expresses the condition (6) of irrotational flow, and the boundary conditions (3)–(5) can be written as

$$v = 0 \quad \text{on} \quad y = -d, \tag{12}$$

$$v = (u-c)\eta_x \quad \text{on} \quad y = \eta(x), \tag{13}$$

and

$$P = \frac{1}{\rho}\mathcal{P}_{\text{atm}} \quad \text{on} \quad y = \eta(x), \tag{14}$$

respectively.

2.1.1. Re-formulation in terms of the stream function. Since the fluid domain

$$\Omega = \{(x, y):\ -d < y < \eta(x)\}$$

is a connected set, it is advantageous to use (9) to reduce the number of unknowns in the governing equations by introducing the *stream function* $\psi(x, y)$ by means of

$$\psi_x = -v, \qquad \psi_y = u - c. \tag{15}$$

Note that (12) and (13) ensure that ψ must be constant on the flat bed $y = -d$ and on the free surface $y = \eta(x)$. Since ψ is uniquely defined up to an additive constant, due to (15), let us set $\psi = 0$ on the free surface and $\psi = m$ on the flat bed, so that

$$\psi(x, y) = m + \int_{-d}^{y} [u(x, s) - c]\, \mathrm{d}s \quad \text{for} \quad -d \leqslant y \leqslant \eta(x).$$

This formula shows that ψ is L-periodic in the x-variable and also clarifies the physical interpretation of the constant

$$m = \int_{-d}^{\eta(x)} [c - u(x, y)]\, \mathrm{d}y$$

as the *relative mass flux* (relative to the uniform flow at constant speed c). In addition to encoding the velocity field by means of (15), the stream function permits us to write the boundary condition (14) in a more transparent way. Indeed, due to (11), one can easily check that (10) is equivalent to the fact that the expression

$$\left[\frac{\psi_x^2 + \psi_y^2}{2} + g(y + d) + P\right]$$

is constant throughout the fluid domain Ω; this being a form of conservation of energy (*Bernoulli's law* for travelling waves). We can now express (14) as the constraint

$$\frac{\psi_x^2 + \psi_y^2}{2\,g} + y + d = Q \quad \text{on} \quad y = \eta(x), \tag{16}$$

for some physical constant Q, called *head*. Note that all the terms in $\frac{\psi_x^2+\psi_y^2}{2\,g} + y + d$ have the dimension of length, the first being called the velocity head and representing the elevation needed for the fluid to reach the velocity $|\nabla\psi|$ during frictionless free fall, and the second term being the height above the flat bed. The equivalent form (16) of (14) does not involve the pressure and its nonlinear character is now plain. Consequently, in terms of the stream function, the governing equations (9)–(14) can be re-formulated as

$$\begin{cases} \Delta\psi = 0 \quad \text{in} \quad -d < y < \eta(x), \\ \psi = 0 \quad \text{on} \quad y = \eta(x), \\ \psi = m \quad \text{on} \quad y = -d, \\ \dfrac{\psi_x^2 + \psi_y^2}{2g} + y + d = Q \quad \text{on} \quad y = \eta(x). \end{cases} \tag{17}$$

This is an over-determined elliptic boundary-value problem: specifying η, the first two boundary conditions in (17) determine ψ throughout the domain. The presence of an additional boundary condition reflects the fact that (17) is a free-boundary problem: the upper boundary of the domain is not known in advance and has to be determined as part of the solution, this being possible because of the additional available constraint. Note that the unknown P is absent from (17). It can be recovered by means of Bernoulli's law, setting

$$P = gQ + \frac{1}{\rho}\,\mathcal{P}_{\text{atm}} - \frac{|\nabla\psi|^2}{2} - g\,(y + d).$$

Indeed, then (14) clearly holds and (10) becomes simply an alternative way to express the gradient of P.

The existence of solutions to (17) is not a trivial matter. For a fixed mean depth $d > 0$, a correlation between the two physical constants m and Q is necessary for the existence of solutions. Even in the absence of waves, for a flat free surface $\eta \equiv 0$, the first three equations in (17) define a Dirichlet problem for the Laplace equation in the strip $\{(x, y):\ -d < y < 0\}$, with the only periodic solution $\psi(x, y) = -\frac{m}{d}y$, so that

$$Q = \frac{m^2}{2gd^2} + d$$

in this case. Other physical flow parameters play also a role, for example the *flow force*

$$F = \int_{-d}^{\eta(x)} \left\{ P(x, y) - \frac{\mathcal{P}_{\text{atm}}}{\rho} + [u(x, y) - c]^2 \right\} \mathrm{d}y;$$

the fact that this expression is independent of the x-variable follows by differentiation, in view of (9), the first component of (10) and (13). Substituting Bernoulli's law into the integrand in the definition of F, one easily obtains the following relation

$$F = gQ\,[\eta(x) + d] - \frac{g}{2}[\eta(x) + d]^2 + \int_{-d}^{\eta(x)} \frac{[u(x, y) - c]^2 - v^2}{2}\mathrm{d}y, \qquad x \in \mathbb{R}.$$

In particular, for the previous flow with a flat free surface we have

$$F = \frac{m^2}{d} + \frac{gd^2}{2}.$$

For given m, Q and F, from the two cubic equations in d that provide the expressions for Q and F we obtain a quadratic equation that yields the two alternative depths

$$d = \frac{F}{gQ} \pm \sqrt{\left(\frac{F}{gQ}\right)^2 - \frac{3}{2}\frac{m^2}{gQ}},$$

known in channel flow theory. It turns out that for waves of small amplitude the three parameters m, Q and F determine the wave train, see [39]. However, for waves of large amplitude, results of this type are not available; see [44] for a discussion of flow-invariants. To illustrate the difficulty, note that no explicit solutions with a non-flat free surface are known. Seeking approximations to the solution by means of a perturbation series in terms of a small parameter, most often the wave steepness, near flows with a flat surface, is an efficient procedure for waves of small amplitude; see the discussion in [30]. For example, at first order we have

$$\eta(x) = \varepsilon \cos(kx) + \mathfrak{O}\left(\varepsilon^2\right),$$

where $\varepsilon > 0$ is the first-order (small) amplitude, $k = \frac{2\pi}{L}$ is the wave number and $\mathfrak{O}(\varepsilon^2)$ stands for an expression with growth rate ε^2. The second-order approximation reads

$$\eta(x) = \varepsilon \cos(kx) + k\varepsilon^2 \frac{3 - \tanh(kd)}{4\tanh^3(kd)} \cos(2kx) + \mathfrak{O}\left(\varepsilon^3\right),$$

where ε is the first-order wave amplitude (see [25]). However, for waves of large amplitude, even if the unknown terms in the expansion in powers of ε can be solved sequentially, the convergence issues impart on the accuracy of the approximation procedure: a non-zero radius of convergence of the power series exists, as shown in [61], but the question of its size remains intractable. Our point of view is that a Stokes wave was generated somehow and we would like to elucidate the main features of the flow pattern beneath it, without limiting our considerations to waves of small amplitude. This endeavor is interesting from a theoretical standpoint and is also practically relevant. For example, the design of cost-effective offshore structures relies on accurate measurements of fluid velocities and pressures beneath the waves. Also, direct wave measurements are often extremely difficult and a widely used approach to convey information about waves is by means of data recorded by pressure sensors or velocitymetres. Modern pressure sensors provide very accurate pressure measurements and by means of modern velocitymetres one can measure with accuracy the fluid velocity at certain locations. However, the conversion of this data into the most important wave characteristics (wave height, wave speed and wave period) is quite delicate, whether the records are performed at fixed positions on the rigid bed or if the instruments are mounted on fixed underwater platforms. Note that the *wave height* is defined as the overall vertical change in height between the wave crest and the wave trough, while the *wave amplitude* is the maximum deviation of the wave profile from the mean surface level $y = 0$; observations of swell indicate that the distance from the crest to the mean surface level usually exceeds that from the trough to the mean surface level (a fact that is consistent with sharper crest elevations and flatter depressions). A good understanding of the flow beneath the waves is essential in trying to come to terms with the wave recovery from subsurface measurements.

For an in-depth discussion of the existence theory for Stokes waves we refer to [10]. Here we only gather some basic facts that are useful in our subsequent considerations. For clarification, given some physical flow parameters d, m, and Q, let us call *Stokes wave* a smooth solution (η, ψ) to (17), having period L in the x-variable and mean level $y = 0$, that is, with

$$\int_0^L \eta(x)\mathrm{d}x = 0. \tag{18}$$

Moreover, there is a single crest and trough per period, and the wave profile η is strictly decreasing from crest to trough, with the solution (η, ψ) symmetric about the crest line (that is, the vertical line directly below a crest, in the moving frame). In terms of the velocity field (u, v) and the pressure P, this means that u and P are symmetric while v is anti-symmetric about the crest line.

Let us now provide some indicative wave characteristics. The wave height of typical ocean swell is about 1.5 m and occasionally it can exceed 5 m. Swell with wavelength 800 m was observed near the south coast of England and in the equatorial Atlantic swell about 900 m long was recorded, see [36], while the shortest wavelengths are about $8 - 9$ m. Swell propagates mostly at speeds in the range from 30 to 70 km h^{-1}, having (temporal) periods in excess of 10 s, over long distances. For example, swell generated by storms between Ireland and Iceland is regularly encountered near Casablanca in Morocco, more than 2500 km away. As for the physical relevance of flows propagating in water with a horizontal bed, the flattest areas on Earth, presenting slopes inferior to 10^{-4}, are the abyssal plains (vast sediment-covered regions of the sea floor resulting from the blanketing of a once irregular topography). These cover almost a third of the Earth's surface (almost as much as all the exposed land combined), and the largest abyssal plains are hundreds of km wide and thousands of km long. For example, the Sohm Plain in the North Atlantic covers an area of about $9 \cdot 10^6$ km^2.

More relevant than the wave height

$$\mathfrak{h} = \eta(0) - \eta(L/2),$$

where $x = 0$ and $x = L/2$ are the locations of the wave crest and of the wave trough, respectively, is the slope η_x of the wave profile. Observations of the *wave steepness*

$$\frac{\mathfrak{h}}{L} = \frac{1}{L}\int_0^{L/2} \eta_x(x)\mathrm{d}x$$

give values up to $1/7 \approx 0.143$; note that the steepness is defined as half of the average slope $\frac{2}{L}\int_0^{L/2} \eta_x(x)\mathrm{d}x$ between a wave crest and its adjacent trough. As the wave steepness increases, nonlinear features become predominant and the wave profile becomes increasingly asymmetric owing to wave-crest steepening and wave-trough flattening. Close to the critical value 1/7 the wave starts to exhibit fore-aft asymmetry because of wave-crest front-face steepening at the onset of breaking, see [52]. Moreover, experimental data and field observations show that for Stokes waves that are not near breaking, the values of the horizontal fluid velocity u throughout the fluid never reach the wave speed c. In our setting, this is captured by imposing the condition

$$u < c \quad \text{throughout the fluid.} \tag{19}$$

To explain (19), note that by Green's theorem and periodicity we have that

$$0 = \int_{-d}^{y_0}\int_0^L (u_y - v_x)\mathrm{d}x\mathrm{d}y = \int_0^L u(x, y_0)\mathrm{d}x - \int_0^L u(x, -d)\mathrm{d}x$$

at all depths y_0 below the trough level $\eta(L/2)$. The fact that the mean of u at any level below the trough is constant signals the presence of a uniform current beneath the waves. The absence of underlying currents is therefore appropriated by requiring that

$$\int_0^L u(x, -d)\mathrm{d}x = 0. \tag{20}$$

In particular, this means that the smooth function u has to vanish somewhere on the flat bed $y = -d$, and knowing that $u \neq c$ throughout the fluid leads us to (19). Another useful consequence of (20) is that it permits the recovery of the wave speed c from the fluid velocity in the moving frame, that is, assuming that $(u - c)$ is known. Indeed

$$c = -\frac{1}{L}\int_0^L [u(x, -d) - c]\,\mathrm{d}x,$$

due to (20), so that the wave speed is the mean of the apparent horizontal fluid velocity at the flat bed, or at any fixed depth below the wave trough level. This is Stokes' first definition of the wave speed, see [59]. Stokes' second definition of the wave speed is to set the wave speed equal to depth-averaged apparent horizontal fluid velocity (in the moving frame), that is, equal to

$$\frac{-1}{Ld}\int_0^L \int_{-d}^{\eta(x)} [u(x, -d) - c]\,\mathrm{d}y\mathrm{d}x = \frac{m}{d}.$$

While within the framework of linear theory the two definitions are consistent, it turns out that

$$c > \frac{m}{d}$$

for a genuine Stokes wave, that is, whenever the free surface is not flat (see [12]). This permits one to calculate the unsteady water velocities in the physical frame through which the waves are moving, from measurements performed on the steady flow in the moving frame.

We would like to point out that several assumptions that were specified in the above definition of a Stokes wave are not restrictive requirements. The free surface must always be a graph, that is, overhanging profiles are not possible, see [65]. Moreover, assuming the free boundary to be a continuously differentiable curve, the boundary must be a real-analytic curve, and the velocity components have harmonic extensions across it (see [62]). Also, the symmetry of the free surface is actually guaranteed if the wave profile is monotone between crests and troughs, see [50], and it is known that $0 < \eta_x^2 < 1$ between consecutive crests and troughs, see [1, 54]. While there exist Stokes waves such that $\eta_x^2 > 1/3$ at some location between crest and trough, a result that gains in significance if compared with the empirical criterion of steepness at most 1/7 mentioned above, the upper bound 1 on the slope is not sharp, but suffices for our purposes. On the other hand, the Stokes wave of greatest height [2, 53], for which the symmetric free surface is not continuously differentiable, fails to satisfy (19) precisely at the crest, where $u = c$ and the profile has a corner with an angle of 120°, see [62]. It is therefore not among the waves we are investigating. Our considerations apply to smooth Stokes waves, up to the wave of greatest height. While the wave of greatest height is obtained mathematically as a limit of smooth Stokes waves, many of its features are far from obvious. For example, while it is indeed the highest travelling wave, it is not the fastest nor the most impulsive nor the most energetic, see [56]. The reasons for excluding the Stokes wave of greatest height from our considerations are not merely technical. The wave of greatest height is associated with incipient wave breaking, and the waves approaching breaking are highly unsteady and deform rapidly, their crest-front faces become very steep and develop an overturning pattern with a forward projected water jet, see [52].

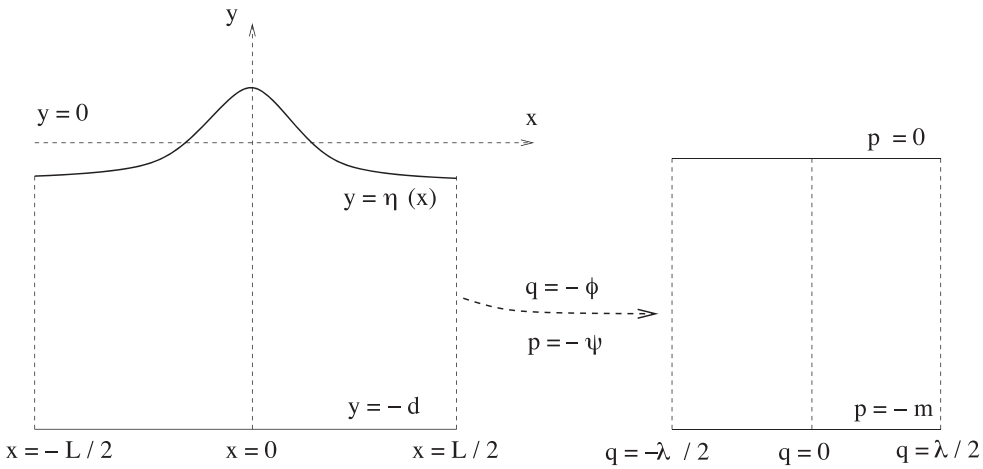

Figure 2. The hodograph transform: inverting the dependent and independent variables, by taking (up to a change of sign) the velocity potential and stream function as the independent variables, and the coordinates (x, y) as the dependent variables, the elliptic free-boundary problem is transformed into an elliptic boundary-value problem in a strip. This has the advantage that the location of the boundary is known beforehand, without being an unknown part of the solution.

2.1.2. Hodograph transform. To fix the conceptual framework, let us assume throughout this paper that the wave crest is located at $(0, \eta(0))$ in the moving frame. The condition (11) of irrotational flow allows us to define the velocity potential $\phi(x, y)$ by

$$\phi_x = u - c, \qquad \phi_y = v. \tag{21}$$

Setting

$$\phi(x, y) = \int_0^x [u(l, -d) - c]\, \mathrm{d}l + \int_{-d}^y v(x, s)\mathrm{d}s, \qquad -d \leqslant y \leqslant \eta(x),$$

we ensure that $\phi = 0$ on the crest line, that is, $\phi(0, y) = 0$ for $y \in [-d, \eta(0)]$. Note that $(x, y) \mapsto \phi(x, y) + cx$ is odd and periodic with period L in the x-variable. In particular, $\phi(jL, y) = -cjL$ for every integer j. Moreover, $\phi_x < 0$ due to (19).

The stream function ψ, defined in section 2.1.1, and the velocity potential ϕ are harmonic conjugate functions, with the complex mapping $x + \mathrm{i}y \mapsto \phi(x, y) + \mathrm{i}\psi(x, y)$ analytic throughout the fluid domain. It is convenient to perform the orientation-preserving conformal hodograph change of variables

$$\begin{cases} q = -\phi(x, y), \\ p = -\psi(x, y), \end{cases} \tag{22}$$

that transforms the free-boundary problem (17) into a nonlinear boundary-value problem for the harmonic function

$$h(q, p) = y + d \tag{23}$$

in a fixed strip (see figure 2).

The transformed boundary-value problem for the unknown height h above the flat bed is

$$\begin{cases} \Delta_{q,p} h = 0 \quad \text{in the strip} \quad -m < p < 0, \\ h = 0 \quad \text{on} \quad p = -m, \\ 2g(Q - h)\left(h_q^2 + h_p^2\right) = 1 \quad \text{on} \quad p = 0, \end{cases} \tag{24}$$

for h even and periodic of period $\lambda = cL$ in the q-variable. Since in our approach, depending on the context, it is advantageous to use either the moving frame or the conformal coordinates, let us record for further use the formulas

$$\begin{cases} \partial_q = h_p\, \partial_x + h_q\, \partial_y, \\ \partial_p = -h_q\, \partial_x + h_p\, \partial_y, \end{cases} \tag{25}$$

and

$$\begin{cases} \partial_x = (c - u)\partial_q + v\, \partial_p, \\ \partial_y = -v\, \partial_q + (c - u)\partial_p, \end{cases} \tag{26}$$

where

$$\begin{cases} h_q = -\dfrac{v}{(c - u)^2 + v^2} = -\dfrac{\partial x}{\partial p} = \dfrac{\partial y}{\partial q}, \\ h_p = \dfrac{c - u}{(c - u)^2 + v^2} = \dfrac{\partial x}{\partial q} = \dfrac{\partial y}{\partial p}, \end{cases} \tag{27}$$

and

$$\begin{cases} c - u = \dfrac{h_p}{h_q^2 + h_p^2}, \\ v = -\dfrac{h_q}{h_q^2 + h_p^2}. \end{cases} \tag{28}$$

2.2. Basic properties of the velocity field

Let us now derive some basic properties of the velocity field beneath a Stokes wave with a non-flat free surface. In the fluid region

$$\Omega_+ = \{(x, y):\ x \in (0, L/2),\ -d < y < \eta(x)\}$$

beneath the free surface $y = \eta(x)$ and above the flat bed $y = -d$, delimited laterally by the crest line $x = 0$ and the trough line $x = L/2$, (9) and (11) ensure that v is a harmonic function. Since $\eta'(x) < 0$ for $x \in (0, L/2)$, from (13) and (19) we infer that $v(x, \eta(x)) > 0$ for $x \in (0, L/2)$. Since $v(x, -d) = 0$ by (12), the strong maximum principle (see [10]) yields that $v > 0$ in the interior of Ω_+. By anti-symmetry, $v < 0$ in the fluid region

$$\Omega_- = \{(x, y):\ x \in (-L/2, 0),\ -d < y < \eta(x)\},$$

obtained by reflection of Ω_+ in the crest line, while $v = 0$ on the crest and trough lines. These considerations provide us with the sign of the vertical fluid velocity component in the moving frame (x, y) in which the flow is steady, and, due to (7)–(8), also when one takes into account variations in time in the physical frame (X, Y) through which the waves are moving; see figure 3.

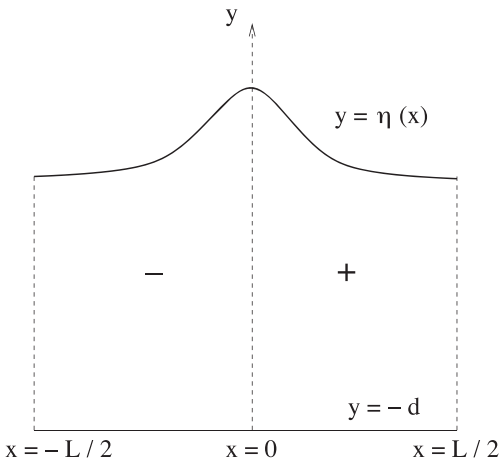

Figure 3. In the moving frame, the vertical velocity component vanishes on the flat bed and on the vertical lines below the wave crest and below the wave trough, having elsewhere a strict sign. In a periodicity window, $v \geqslant 0$ in the fluid domain beneath the descending part of the wave profile, while $v \leqslant 0$ in the fluid domain beneath the ascending part of the wave profile.

To deal with the horizontal fluid velocity, let us first observe that a direct calculation based on (10) yields that P is superharmonic throughout the fluid region Ω, as

$$\Delta P = -\psi_{xx}^2 - 2\psi_{xy}^2 - \psi_{yy}^2 \leqslant 0.$$

Since P is periodic in the x-variable and $P_y = -g < 0$ on $y = -d$, in view of (12) and the second component of the Euler equation (10), Hopf's maximum principle (see [10]) ensures that the minimum of P in the closure of Ω is attained only on the free surface $y = \eta(x)$, along which P is constant due to (14). Furthermore, the fact that $\eta_x(x) < 0$ for $x \in (0, L/2)$ means that along the upper boundary of Ω_+ the positive x-direction points outwards, and therefore $P_x(x, \eta(x)) < 0$ for all $x \in (0, L/2)$, again by Hopf's maximum principle. Taking into account the first component of (10), this means that

$$[u(x, \eta(x)) - c]\, u_x(x, \eta(x)) - v(x, \eta(x)) u_y(x, \eta(x)) > 0, \quad x \in (0, L/2).$$

Expressing the above inequality in (q, p)-coordinates by means of (26) yields

$$u_q(q, 0) < 0 \quad \text{for} \quad q \in (0, \lambda/2).$$

On the other hand, since $v = 0$ on the crest and trough lines and (9) ensure $u_x = v_y = 0$ on the crest and trough lines, (26) also yields

$$u_q(0, p) = u_q(\lambda/2, p) = 0 \quad \text{for} \quad p \in [-m, 0].$$

Furthermore, from (26), (12) and (9) we get

$$u_q(q, -m) = \frac{u_x(x, -d)}{c - u(x, -d)} = -\frac{v_y(x, -d)}{c - u(x, -d)},$$

where the point $(q, -m)$ corresponds to $(x, -d)$ under the change of variables (22). Knowing that the harmonic function v attains its minimum in Ω_+ along the lower flat boundary $y = -d$, we infer by Hopf's maximum principle that $v_y(x, -d) > 0$ for $x \in (0, L/2)$, so that

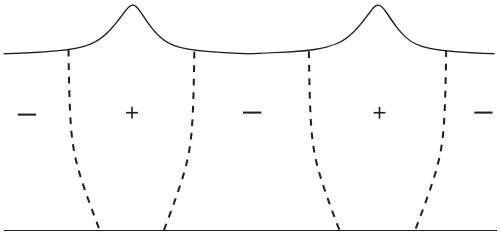

Figure 4. In a periodicity window of the moving frame, the horizontal velocity component vanishes along two smooth curves that connect the free surface to the flat bed, being strictly positive in the fluid region beneath the wave crest and strictly negative in the fluid region beneath the wave trough. The fact that the curves bend as indicated in the figure is hypothetical: currently it is known that each streamline ($\psi =$ constant) intersects such a curve in precisely one point, and that each curve lies between adjacent crest and trough lines without intersecting them.

$$u_q(q, -m) < 0 \quad \text{for} \quad q \in (0, L/2).$$

Denoting by

$$\widehat{\Omega}_- = \left\{(q, p):\ -\frac{\lambda}{2} < q < 0,\ -m < p < 0\right\},$$
$$\widehat{\Omega}_+ = \left\{(q, p):\ 0 < q < \frac{\lambda}{2},\ -m < p < 0\right\},$$

the images of the regions Ω_- and Ω_+ under the conformal change of variables (22), the previous considerations show that $u_q \leqslant 0$ all along the boundary of $\widehat{\Omega}_+$, with strict inequality at places on the upper and lower boundary. Since u was harmonic in the (x, y)-coordinates and a conformal change of variables preserves harmonicity, u will be harmonic in $\widehat{\Omega}_+$. The strong maximum principle (see [10]) is therefore applicable and we conclude that

$$u_q < 0 \quad \text{throughout} \quad \widehat{\Omega}_+.$$

Now, (20) and symmetry yield $\int_0^{L/2} u(x, -d)\mathrm{d}x = 0$. In combination with the established fact that $u_x(x, -d) < 0$ for $x \in (0, L/2)$, this permits us to infer the existence of a unique point $x_0 \in (0, L/2)$ with $u(x_0, -d) = 0$. Consequently, there exists a unique point $q_0 \in (0, \lambda/2)$ with $u(q_0, -m) = 0$. Since $u_q(q, -m) < 0$ for $q \in (0, \lambda/2)$, we obtain that $u(q, -m) > 0$ for $q \in [0, q_0)$ while $u(q, -m) < 0$ for $q \in (q_0, \lambda/2]$. Let us now take advantage of the fact that v is harmonic in $\widehat{\Omega}_+$ and attains its minimum there all along the lateral sides of $\widehat{\Omega}_+$, both properties being inherited from its behaviour in Ω_+. Therefore, Hopf's maximum principle yields $v_q(0, p) > 0 > v_q(\lambda/2, p)$ for $p \in (-m, 0)$. Since $u_p = v_q$, as a glance at (26) in combination with (9) and (11) will confirm, we deduce that

$$u_p(0, p) > 0 > u_p(\lambda/2, p) \quad \text{for} \quad p \in (-m, 0).$$

As a useful consequence, the inequality $u(0, -m) > 0 > u(\lambda/2, -m)$ enforces

$$u(0, p) > 0 > u(\lambda/2, p) \quad \text{for} \quad p \in [-m, 0].$$

A streamline in the moving frame is a level set of ψ and corresponds in (q, p)-coordinates to a horizontal line. Along the horizontal segment in which such a line intersects $\widehat{\Omega}_+$ we know that $u_q < 0$, while $u > 0$ at the left endpoint and $u < 0$ at the right endpoint. Consequently u

vanishes on this segment at precisely one point. By reflection in the line $q = 0$, a mirror image of this occurs in $\widehat{\Omega}_-$. Note that if we denote by $(\alpha(p), p)$ the points in $\widehat{\Omega}_+$ where u vanishes, since $u_q < 0$ throughout $\widehat{\Omega}_+$, the implicit function theorem ensures that $p \mapsto \alpha(p)$ is a smooth curve. Its pre-image under the change of variables (22) will therefore be a smooth curve in Ω_+, connecting the upper boundary $y = \eta(x)$ to the flat lower boundary $y = -d$ by intersecting each streamline precisely once; see figure 4.

2.3. The particle path pattern

The trajectory $t \mapsto (X(t), Y(t))$ of a fluid particle with initial position (X_0, Y_0), as the wave propagates, is of great interest in understanding the flow beneath the waves. Information about its behaviour has to be extracted from the time-dependent system

$$\begin{cases} X' = U(X - cT, Y), \\ Y' = V(X - cT, Y), \end{cases} \tag{29}$$

with initial data $(X(0), Y(0)) = (X_0, Y_0)$. The ordinary differential equations (29) simply express the fact that velocity is the rate of change of the displacement. Due to the lack of explicit solutions for Stokes waves with a non-flat surface, it is quite natural to try to investigate the particle trajectories by means of approximations. First-order linear theory gives the leading order

$$\begin{cases} U(X - cT, Y) = \varepsilon kc \dfrac{\cosh[k(Y + d)]}{\sinh(kd)} \cos[k(X - cT)], \\ V(X - cT, Y) = \varepsilon kc \dfrac{\sinh[k(Y + d)]}{\sinh(kd)} \sin[k(X - cT)], \end{cases} \tag{30}$$

of the velocity field beneath the linear wave profile $\varepsilon \cos[k(X - cT)]$, propagating at speed $c = \sqrt{g \frac{\tanh(kd)}{k}}$; see [10] for details. Note that, despite the linearization of the governing equation, the nonlinear character of the system corresponding to (29) persists. For this reason, nelecting terms of second order in the power series expansion of the velocity field (30) in the small parameter ε, we end up with the linear system

$$\begin{cases} X'(T) = \varepsilon kc \dfrac{\cosh\left[k\left(Y_0 + d\right)\right]}{\sinh(kd)} \cos\left[k\left(X_0 - cT\right)\right], \\ Y'(T) = \varepsilon kc \dfrac{\sinh\left[k\left(Y_0 + d\right)\right]}{\sinh(kd)} \sin\left[k\left(X_0 - cT\right)\right]. \end{cases} \tag{31}$$

The explicit solution to (31) with initial data $(X(0), Y(0)) = (X_0, Y_0)$ is

$$\begin{cases} X(T) = X_0 + \varepsilon \dfrac{\cosh\left[k\left(Y_0 + d\right)\right]}{\sinh(kd)} \Big(\sin\left(kX_0\right) - \sin\left[k\left(X_0 - cT\right)\right] \Big), \\ Y(T) = Y_0 + \varepsilon \dfrac{\sinh\left[k\left(Y_0 + d\right)\right]}{\sinh(kd)} \Big(\cos\left[k\left(X_0 - cT\right)\right] - \cos\left(kX_0\right) \Big). \end{cases} \tag{32}$$

Consequently, to a first-order approximation, a water particle located initially at (X_0, Y_0) above the flat bed $Y = -d$ will describe clockwise an elliptic orbit, the centre of the ellipse being

$$\left(X_0 + \varepsilon \frac{\cosh\left[k\left(Y_0+d\right)\right]}{\sinh\left(kd\right)} \sin\left(kX_0\right),\ Y_0 - \varepsilon \frac{\sinh\left[k\left(Y_0+d\right)\right]}{\sinh\left(kd\right)} \cos\left(kX_0\right) \right),$$

while the lengths of the horizontal major axis and of the vertical minor axis of the ellipse are $\frac{2\varepsilon \cosh\left[k\left(Y_0+d\right)\right]}{\sinh\left(kd\right)}$ and $\frac{2\varepsilon \sinh\left[k\left(Y_0+d\right)\right]}{\sinh\left(kd\right)}$, respectively. All these ellipses have the same eccentricity (distance between their foci) $\frac{\varepsilon}{\sinh\left(kd\right)}$, but the lengths of both their axes decrease as we go downward into the water, and at the bottom the ellipse degenerates into a straight line. Each particle appears to describe its ellipse in a wave period, and they are all in the same phase.

Support for the particle trajectory pattern predicted by linear theory seems to be given by some early films of small buoyant particles in laboratory wave tanks, where closed elliptical paths appear to be recognizable (see [4]), with various photographs reproduced in standard textbooks on water waves [24, 57, 58]. However, one should have serious reservations about the approach described above. Other than the issue of convergence of the power series expansions that underlie the procedure, recall that the explicit system (29) with the right-hand given by (30), describing the motion of the particles within the framework of linear wave theory, is nevertheless nonlinear and a further linearization was performed. The obtained closed orbits throughout the flow represent a highly regular pattern that is easily destroyed by small perturbations, so that it is unlikely that this outcome is realistic. As a matter of fact, if one refrains from linearizing (30), it turns out that the particle paths are no longer closed, see [21, 33], and each particle performs a back-and-forth motion but experiences a net forward drift, in the direction of wave propagation. Moreover, relying (formally) on quadratic quantities in the wave amplitude within the framework of linear theory, one can compute the average flow of energy beneath a Stokes wave and infer that the fluid experiences on average a net displacement in the direction in which the waves are propagating; see the discussion in [41]. A more detailed analysis is therefore desirable. We could try to go beyond the first-order approximation of the free surface, but this type of approach is contingent on the convergence of the power series expansions and will therefore be only valid for waves of very small amplitude. Pursuing an analysis of model equations (like KdV) that are encountered in soliton theory is not an option since these model equations are always derived for waves of small amplitude and they are valid approximations in the shallow-water regime in which vertical variations of the fluid velocity are neglected (see the discussion in [10, 31]). Relying on the guiding principle that waves of moderate and large amplitude hold few surprises, and that the insight provided by studies of waves of small amplitude reveals the main structure of the flow field, is a questionable point of view. It turns out that the lack of explicit solutions is compensated by a rich structure that can be exploited to reduce the complexity of the problem by qualitative rather than quantitative means, drawing conclusions that are valid for waves of small and large amplitude. We follow closely the considerations made in [9, 17].

The system corresponding to (29) in the moving frame is the autonomous differential system

$$\begin{cases} x' = u(x,\, y) - c, \\ y' = v(x,\, y), \end{cases} \tag{33}$$

with initial data $(x(0),\, y(0)) = (X_0,\, Y_0)$; in (33) the time variable is $t = T$. By the definition of the stream function, the system (33) is Hamiltonian with Hamiltonian function ψ, so that

$$\psi\left(x(t),\, y(t)\right) = \psi\left(X_0,\, Y_0\right) \quad \text{for all times} \quad t,$$

a fact that can also be checked directly. Moreover, the periodicity of u in the x-variable and (19) ensure the existence of some $\delta > 0$ such that $u(x,\, y) - c \leqslant -\delta$ for all $(x,\, y) \in \Omega$.

Consequently, as t runs from $-\infty$ to ∞, $x(t)$ will run from ∞ to $-\infty$. Thus, without loss of generality, we may assume that $x(0) = L/2$. We call *elapsed time* the positive time $\tau = \tau(Y_0) > 0$ when $x(t) = -L/2$: this is the time it takes $(x(t), y(t))$ to traverse one periodicity window, from trough line to trough line, in the moving frame. If we denote by $(q(t), p(t))$ the location of the image of the point $(x(t), y(t))$ under the conformal map (22), then $p(t) = p$ is an integral of motion, since $(x(t), y(t))$ stays on the same streamline, while the definition of the velocity potential and (33) yield

$$\frac{\mathrm{d}q}{\mathrm{d}t} = q' = -\phi_x x' - \phi_y y' = -(c-u)^2 - v^2 \leqslant -\delta^2,$$

with $q(0) = \lambda/2$ and $q(\theta) = -\lambda/2$, so that the motion of $(q(t), p(t))$ occurs on straight horizontal lines, from right to left in the (q, p)-plane; here $\theta(p) = \tau(Y_0)$. Consequently

$$y(\tau) - y(0) = \int_0^\tau v(x(t), y(t))\mathrm{d}t = \int_{-\lambda/2}^{\lambda/2} \frac{v}{(c-u)^2 + v^2}\mathrm{d}q = 0$$

since v is odd and u is even in the q-variable, while

$$\theta(p) = \int_0^\theta \frac{x'(t)}{u(x(t), y(t)) - c}\mathrm{d}t = \int_{-L/2}^{L/2} \frac{\mathrm{d}x}{c - u(x, y(x))}, \tag{34}$$

where $y = y(x)$ is the streamline to which (X_0, Y_0) belongs to. The divergence theorem applied to the function $(v, c-u)$ in the region beneath the streamline $y = y(x)$ and above the flat bed $y = -d$, delimited laterally by the trough lines $y = \pm L/2$, yields

$$cL = \int_{-L/2}^{L/2} (c - u(x, y(x)))\sqrt{1 + \left[y_x(x)\right]^2}\,\mathrm{d}x \tag{35}$$

in view of (11), (20) and the periodicity in the x-variable, since by differentiation of the relation $\psi(x, y(x)) = p$ with respect to the x-variable we get

$$y_x(x) = -\frac{v(x, y(x))}{c - u(x, y(x))}.$$

Note that the sign of v in conjunction with (19) ensure that all streamlines except the flat bed $y = -d$ replicate the shape of the free surface in the moving frame: they are smooth, symmetric curves that are strictly decreasing between a wave crest and the adjacent trough. By the Cauchy–Schwarz inequality we have

$$L^2 \leqslant \int_{-L/2}^{L/2} \frac{\mathrm{d}x}{c - u(x, y(x))} \int_{-L/2}^{L/2} (c - u(x, y(x)))\mathrm{d}x.$$

For all streamlines except the flat bed $y = -d$ we have that $y_x(x) = 0$ can only occur at the intersection with a crest line or with a trough line, so that

$$\int_{-L/2}^{L/2} (c - u(x, y(x)))\sqrt{1 + \left[y_x(x)\right]^2}\,\mathrm{d}x > \int_{-L/2}^{L/2} (c - u(x, y(x)))\mathrm{d}x.$$

Combining this with the inequality displayed above it yields, in view of (34),

$$\theta(p) > \frac{L}{c}, \qquad p \in (-m, 0].$$

The above estimate for the elapsed time holds also for $p = -m$. Indeed, while in this case $y_x \equiv 0$ prevents us from relying on the same argument, the possible equality for $p = -m$ is ruled out by the fact that, since $\int_{-L/2}^{L/2} (c - u(x-d))\mathrm{d}x = cL$ by (20), it would entail equality in the Cauchy–Schwarz inequality. This, in its turn, would force u to be constant on the flat

bed, and we know that this is not the case. Consequently

$$\theta(p) > \frac{L}{c}, \qquad p \in [-m, 0], \tag{36}$$

We now define the *particle drift* $\mathfrak{D} = \mathfrak{D}(Y_0)$ as the net horizontal distance moved by the particle between its positions below two consecutive troughs, that is

$$\mathfrak{D} = X(\tau) - X(0) = c\,\theta - L, \tag{37}$$

since $X(T) = x(t) + ct$ and in time $\tau = \theta$ the solution $(x(t), y(t))$ to (33) moves from the trough line $x = L/2$ to the trough line $x = -L/2$ in the moving frame. Zero drift singles out the closed paticle paths. Indeed, only at integers multiples of θ is the y-coordinate of the solution $(x(t), y(t))$ to (33) equal to Y_0, and $X(n\tau) - X(0) = n[X(\tau) - X(0)]$ for an integer n, so that a return of the solution $(X(t), Y(t))$ of the system (29) to the initial position (X_0, Y_0) is only possible if $\mathfrak{D}(Y_0) = 0$. Furthermore, if $\mathfrak{D}(Y_0) = 0$, then $X(\tau) = X(0)$, $Y(\tau) = Y(0)$ and $\tau = L/c$, so that the periodicity of the velocity field in the X-variable ensures that $t \mapsto (X(t), Y(t))$ as well as $t \mapsto (X(t + \tau), Y(t + \tau))$ solve (29) with the same initial data. The velocity field (U, V) being real-analytic, we have uniqueness of solutions, that is, $X(t + \tau) = X(t)$ and $Y(t + \tau) = Y(t)$ for all $t \in \mathbb{R}$. Since (36) ensures a positive drift, we conclude that there are no closed particle paths. The previous considerations enable us to provide a qualitative description of the particle trajectories above the flat bed. For this, recall that by(36) and (37), the drift of any particle is positive. The properties of u proved in section 2.2 show that in Ω_+ the level set $[u = 0]$ consists of a continuous curve $\mathcal{C}_+$ that intersects each streamline $[\psi = -p]$ with $p \in [-m, 0]$ exactly once, while in Ω_- the level set $[u = 0]$ is obtained by reflecting the curve $\mathcal{C}_+$ in the vertical line $x = 0$, obtaining a smooth curve $\mathcal{C}_-$. The two curves $\mathcal{C}_\pm$ delimit laterally the fluid region (in the moving frame) where $u > 0$ (including the top and lower boundaries), while between the trough line $x = -L/2$ and the curve $\mathcal{C}_-$ and between the curve $\mathcal{C}_+$ and the trough line $x = L/2$ we have that $u < 0$. In particular, $u < 0$ on the trough line and $u > 0$ on the crest line. In the moving frame, the particle located initially at the point A, of elevation $Y_0 > -d$ on the trough line $x = L/2$, reaches the trough line $x = -L/2$ in time $\theta = \theta(Y_0)$, with $y(\theta) = Y_0$. As t progresses through the time interval $(0, \theta)$, the path $(x(t), y(t))$ will successively intersect the curve $\mathcal{C}_+$ at a point B, the crest line $x = 0$ at a point C, then curve $\mathcal{C}_-$ at a point D, until it finally intersects the trough line $x = -L/2$ at $E = (-L/2, Y_0)$, at the instant $t = \theta$. Since $u < 0$ while $(x(t), y(t))$ travels in the moving frame from A to B and from D to E, the corresponding displacement $(X(t), Y(t))$ of the particle in the physical variables (X, Y) must be backwards. In the time interval needed for $(x(t), y(t))$ to get in the moving frame from B to D, it lies in the region where $u > 0$, so that $(X(t), Y(t))$ moves forward. Moreover, while $(x(t), y(t))$ travels from A to C we have that $v > 0$, so that $(X(t), Y(t))$ moves up, while $v < 0$ between C and E means that $(X(t), Y(t))$ moves down. The initial position being $(X(0), Y(0)) = (L/2, Y_0)$, while $(X(\theta), Y(\theta)) = (-L/2 + c\theta, Y_0)$, since $x(t) = X(t) - ct$, we have $X(\theta) > L/2 = X(0)$ by (36). Thus E is strictly to the right of A and therefore the particle $(X(t), Y(t))$ describes in the physical frame (X, Y) a loop, as depicted on the top of figure 5. This applies to all particles that are located initially above the flat bed.

As for a particle located on the flat bed $Y = -d$, observe that the boundary condition (12) ensures that it will always move horizontally. Choosing the location $(L/2, -d)$ below the wave trough as a starting point, the particle oscillates in a backward–forward–backward pattern with a net forward drift, mirroring the projection of the loop on the top of figure 5 to the flat bed.

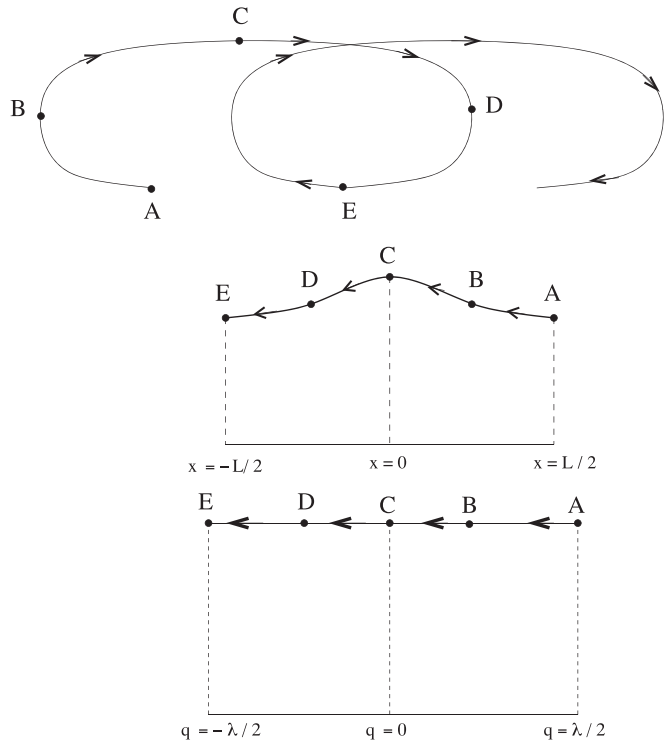

Figure 5. The trajectory of a particle located above the flat bed: in the physical frame (top), in the moving frame (middle) and in the conformal frame (bottom). At C the wave crest is located right above the particle, while at A and E the wave trough is right above it. In the middle and bottom figures, the flat bed is also drawn.

These theoretical predictions were confirmed numerically [49] and experimentally [5, 63]. During this process it became apparent that the size of the particle drifts can be very small for specific wave characteristics. In particular, the experimental photographic evidence reproduced in [24, 57, 58], that seemed to indicate closed particle paths, corresponds to very small drift.

2.4. Basic properties of the pressure

Let us now show that, see [17], in the moving frame the normalized pressure P decreases horizontally away from the crest line towards the adjacent trough line, being strictly increasing with depth. More precisely,

- $P_x < 0$ in the closure $\overline{\Omega_+}$ of the open fluid region Ω_+ and $P_x > 0$ in $\overline{\Omega_-}$, except on the crest line $x = 0$ and on the trough lines $x = \pm L/2$, where $P_x = 0$;
- $P_y < 0$ throughout the entire fluid domain.

In particular, the maximum of the pressure is attained at the point on the flat bed directly below the wave crest, while the minimum of the pressure is attained all along the free surface $y = \eta(x)$.

The first claim follows by the characterization of the sign of u_q in the moving frame (see section 2.2) since combining the first component of (10) with (28) and (26) yields

$$P_x = (c-u)u_x - vu_y = \frac{h_p u_x + h_q u_y}{h_q^2 + h_p^2} = \frac{u_q}{h_q^2 + h_p^2}.$$

To prove the second claim, let us introduce the function

$$f\colon \Omega \to \mathbb{R}, \qquad f(x,y) = (c-u)v - gx.$$

Since u and v are harmonic and (9) as well as (11) hold, one can easily check by directly calculating $\Delta_{(x,y)} f$ that f is harmonic. The change of variables (22) being conformal, we infer that

$$F\colon R = \left\{(q,p)\colon\ -\frac{\lambda}{2} < q < \frac{\lambda}{2},\ -m < p < 0\right\} \to \mathbb{R}, \quad F(q,p) = f(x,y),$$

is also harmonic. Using (26), (27), (9) and (11), we compute

$$F_q = v_x - \frac{g(c-u)}{(c-u)^2 + v^2}. \tag{38}$$

Since $v = v_x = 0$ on the lower boundary of R, due to (12), (19) and (38), we have that

$$F_q(q,-m) < 0 \quad \text{for} \quad -\frac{\lambda}{2} \leqslant q \leqslant \frac{\lambda}{2}. \tag{39}$$

On the lateral boundaries of the rectangle R, obtained as images of the trough lines $x = \pm L/2$ under the conformal map (22), we know that $v = 0$ and $v_x \leqslant 0$ (see section 2.2). Therefore (19) and (38) yield

$$F_q\left(\pm\frac{\lambda}{2}, p\right) < 0 \quad \text{for} \quad -m \leqslant p \leqslant 0. \tag{40}$$

Let us now show that on the upper boundary of the rectangle R we have

$$F_q(q,0) \leqslant 0 \quad \text{for} \quad -\frac{\lambda}{2} \leqslant q \leqslant \frac{\lambda}{2}. \tag{41}$$

For this, multiplying both sides of the last relation in (17) by g and subsequently differentiating with respect to the x-variable, we get

$$\begin{aligned} 0 &= (u-c)\left(u_x + u_y\eta_x\right) + v\left(v_x + v_y\eta_x\right) + g\eta_x \\ &= (u-c)u_x + u_y v + vv_x + (u-c)v_y\eta_x^2 + g\eta_x \\ &= v_y(c-u)\left(1-\eta_x^2\right) - 2(c-u)v_x\eta_x + g\eta_x \ \text{ on } \ y = \eta(x), \end{aligned}$$

using (13) as well as (9) and (11). Since $\eta_x(x) < 0$ for $x \in (0, L/2)$, division of the previous identity by η_x leads us to

$$0 = (c-u)\left(\frac{v_y}{\eta_x}\left(1-\eta_x^2\right) - 2v_x\right) + g \ \text{ on } \ y = \eta(x) \ \text{ with } \ 0 < x < \frac{L}{2}.$$

We know that $\eta_x^2 < 1$ and $\frac{v_y}{\eta_x} < v_x$ on $y = \eta(x)$ for $0 < x < L/2$, the latter since on this part of the free surface

$$0 > u_q = \frac{-v_y + \eta_x v_x}{(c-u)\left(1+\eta_x^2\right)},$$

with the expression of u_q obtained by combining (25), (27), (13), (9), and (11). The previous two displayed relations together with (19) yield

$$0 > -(c-u)\Big(1+\eta_x^2\Big)v_x + g \quad \text{on} \quad y=\eta(x) \quad \text{with} \quad 0<x<\frac{L}{2}.$$

This is precisely the strict inequality in (41) for $0<q<\lambda/2$, due to (38) and (13). Since by (38) F_q is even in the q-variable, the validity of the strict inequality in (41) is also verified for $-\lambda/2<q<0$. Continuity now confirms (41).

The inequalities (39), (40) and (41) for the boundary values of the harmonic function F_q ensure by the strong maximum principle that $F_q<0$ in R, that is

$$v_x < \frac{g(c-u)}{(c-u)^2+v^2} \quad \text{in} \quad R. \tag{42}$$

On the other hand, in section 2.2 we established that

$$0 > u_q = \frac{(c-u)u_x - vu_y}{(c-u)^2+v^2} \quad \text{in} \quad \Omega_+.$$

Using (9), (11) and (19), we infer from the above that

$$v_y > \frac{v}{u-c}v_x \quad \text{in} \quad \Omega_+. \tag{43}$$

Since $v>0$ in Ω_+, as shown in section 2.2, the second component of (10) in combination with (42) and (43) yield

$$P_y = -g + (c-u)v_x - vv_y < -g + \frac{v_x}{c-u}\Big[(c-u)^2+v^2\Big] < 0 \ \text{ in } \ \Omega_+.$$

This proves the validity of the second claim throughout the open set Ω_+. By symmetry, the inequality will also hold in Ω_-. On the trough lines $x=\pm L/2$ we have $v=0$, so that the second component of (10) yields $P_y=(c-u)v_x-g=(c-u)F_q<0$ by (40) and (19), while $P_y(0,y)<0$ for $-d<y<\eta(0)$ since this part of the crest line $x=0$ is included in the rectangle R, and thus $P_y=(c-u)v_x-g=(c-u)F_q<0$ in view of (19) and the fact that $F_q<0$ throughout R. Since $v=v_x=0$ on the flat bed $y=-d$, the second component of (10) becomes $P_y=-g$ there. As for the free surface $y=\eta(x)$, all along it the superharmonic function P attains its minimum in Ω, so that Hopf's maximum principle ensures that $P_y<0$ here as well. By periodicity $P_y<0$ holds throughout the fluid domain.

3. Discussion

The results presented in section 2 describe the basic qualitative features of the flow beneath a Stokes wave with no underlying currents. It is of interest to refine these results and also to investigate in detail the flow pattern in the case of wave–current interactions. In this section we survey some promising recent results in these directions and we specify a number of scenarios that are likely to occur, as indicated by numerical simulations and experimental data.

3.1. Some open problems for waves with no underlying current

For a better understanding of the flow pattern beneath a Stokes wave with no underlying current, the following aspects should be satisfactorily understood.

- The monotonicity properties of the vertical velocity component v are unknown. Numerical simulations [7] suggest that v has a unique maximum along any streamline in Ω_+, but a theoretical confirmation is not available.

- While the results in section 2.2 show that the horizontal velocity component u is strictly decreasing along any streamline in Ω_+, its monotonic behaviour in the vertical and horizontal directions is not yet clarified.
- The horizontal and vertical accelerations are important flow characteristics and no results about their growth pattern are available for waves of large amplitude. For numerical simulations we refer to [7].
- A more detailed theoretical analysis of the looping particle trajectories depicted in figure 5 should be within reach. One can prove (see [17]) that the drift of the particle (the distance from A to E, in figure 5) and the amplitude of the vertical oscillation of a particle (the distance from C to the horizontal line through A and E) are both strictly decreasing with increasing depth. The extent of the forward–backward oscillation of a particle (the distance from B to D) appears to also present this feature, but this fact has eluded a theoretical confirmation.
- Concerning the pressure, it is of interest to investigate its monotonicity along streamlines in the moving frame. Also, the monotonicity of the dynamic pressure, defined as the difference $\mathcal{P} - [\mathcal{P}_{\text{atm}} - \rho g y]$ between the pressure and the hydrostatic pressure, in the vertical and horizontal directions, but also along streamlines, is not clarified.

A special topic of interest concerns the wave of greatest height. It turns out that the particle path pattern depicted in figure 5 persists, as do those of the signs of u and v in the moving frame, see [11]. The approach presented in section 2 can not be implemented due to the failure of (19) at the wave crest, where $u = c$. Nevertheless, it is still relevant since the conclusions for the wave of greatest height can be obtained by a limiting procedure from those valid for waves of almost greatest height, and useful information about the boundary behaviour of the analytic map $q + \mathrm{i}p \mapsto x + \mathrm{i}y$ near the singular point at the wave crest can be extracted. Despite these similarities, there are unexpected features. At first sight, the fact that $u = c$ and $v = 0$ at the wave crest might indicate that the wave crest is a stagnation point of the flow, so that a particle located there (in the physical frame) moves horizontally at the wave speed, remaining at the wave crest. However, the wave crest of a wave of greatest height is only an apparent stagnation point of the flow—no particle can rest there, see [11]. On the other hand, the question of the monotonicity properties of the pressure beneath a wave of greatest height has not been yet investigated. Also the aspects that are not fully understood for the flow beneath regular Stokes waves, listed above, are open for investigation in the context of the wave of greatest height.

3.2. State-of-the-art for wave–current interactions

For periodic two-dimensional travelling waves propagating at the surface of water with a flat bed in a flow with underlying currents, the flow pattern beneath the waves is to a large extent unexplored. Even the case of waves of small amplitude, setting in which perturbation results and linear theory are applicable, offers a few challenges.

The simplest setting is that of an irrotational flow, in which case the underlying current is uniform. While the behaviour of the sign of v and the montonocity properties of the pressure in the vertical and horizontal directions, discussed in section 2, remain unchanged, there is a significant change in the behaviour of the sign of u, namely, the curve $\mathcal{C}_+$ that represents the level set $[u = 0]$ in Ω_+ might be strongly deformed by the underlying current into a curve that no longer connects the free surface to the flat bed, but is now a curve that connects the free surface to the trough line or to the crest line. These possibilities trigger the appearance of new types of particle trajectories: below the lowest point of $\mathcal{C}_+$ the lack of change of sign of u

means that in the horizontal movement of a particle located there is no change of direction, so that the particle moves either in the direction of wave propagation (this will be the case for a favourable current) or opposite to it (for strong adverse currents), propagating as a vertical oscillation due to the change of sign of v. Moreover, in the region where a change of sign in u occcurs a closed particle path might appear at a specific depth. See [17] for theoretical results and [49] for numerical simulations. In addition to the open questions formulated in the absence of underlying currents in section 3.1, the most pressing point is the lack of criteria that specify the strength of the current that triggers the appearance of these new types of particle paths.

The hallmark of non-uniform underlying currents is the presence of vorticity: (11) no longer holds. Instead, we allow for non-zero vorticity $\omega = u_y - v_x$ in the flow beneath the surface waves. The vorticity of a particle is preserved as the particle moves about (see [10]). The simplest rotational setting is that of linearly sheared currents of constant nonzero vorticity, a setting that is regarded as appropriate for the description of tidal currents. These are the alternating horizontal movements of water associated with the rise and fall of the tide: the current associated with a rising tide is called the flood, and the current associated with a falling tide is called the ebb; tides refer to the vertical motion of water (the rise and fall of the tide) caused by the gravitational forces due to the relative motions of Moon, Sun, and Earth. Tidal currents are considered to be the most regular and predictable currents and in many coastal inlets they are the most significant currents. Positive constant vorticity $\omega > 0$ is appropriate for the ebb current and negative constant vorticity $\omega < 0$ is appropriate for the flood current, cf the discussion in [10]. As for the setting of non-constant vorticity, let us point out that the prime source of some ocean currents are long-duration winds and constant vorticity does not give a good description of these currents, a depth-dependent vorticity being more adequate. Also, the out-flowing current at the mouth of an estuary generally exhibits a nonuniform vorticity distribution, see [35].

The first main issue that needs to be addressed theoretically is a re-formulation of the governing equations as a boundary-value problem in a fixed domain rather than as a free-boundary problem. The validity of (9) for rotational waves ensures the existence of a stream function ψ but since (11) fails, there does not exist a velocity potential. While often the separation of the wave–current interaction into a background pure current, corresponding to a rotational flow with a flat free surface, and a superimposed irrotational wave motion is advocated, this type of approach neglects from the start strong interactions between the waves and the current and is therefore not advisable for the study of waves of moderate or large amplitude.

In the absence of stagnation points, one can obtain a suitable change of coordinates (q, p) somewhat analogous to (22) by setting $q = x$ and $p = -\psi$. This semi-hodograph transform, pioneered in [26], fails to be conformal, so that instead of the Laplace equation in the formulation that replaces (24), one obtains a nonlinear elliptic partial differential equation for $h = y + d$. Nevertheless, this transformation can be used to establish the existence of waves of large amplitude [16], to prove regularity [15, 69], and to show that waves with profiles that are monotone between adjacent crests and troughs have to be symmetric [14]. Moreover, for waves of small amplitude a description of the particle paths is possible (see [28]). While results for the particle paths and for the pressure beneath waves of large amplitude are not yet available, let us point out that numerical simulations indicate that the presence of vorticity might alter the fact that the pressure beneath the surface waves is strictly increasing with depth [37].

To capture the presence of stagnation points, an alternative approach was pursued in [40, 66] by using the change of variables $(x, y) \mapsto \left(x, \frac{d+y}{d+\eta(x)}\right)$ that maps the fluid domain (in the moving frame) into a fixed strip. In this case the structure loss is even greater, as one obtains an even more intricate elliptic partial differential equation than it was the case for the semi-hodograph transform. This lack os structure precludes the possibility of pursuing an in-depth analysis of waves of large amplitude. Nevertheless, this approach has the advantage of being applicable for waves of small amplitude in flows with stagnation points. The flow pattern beneath the waves now presents closed streamlines in the moving frame, a feature that is not encountered in irrotational flows.

In the setting of constant non-zero vorticity, a re-formulation of the governing equations as a boundary-value problem in a fixed strip is possible by means of conformal maps [19, 20], and the preservation of harmonicity in this process offers possibilities for an analysis of the flow pattern beneath such waves, without necessarily restricting the considerations to waves of small amplitude. The existence of waves of large amplitude in flows with constant non-zero vorticity was recently established [19], allowing even for the overhanging wave profiles that are observed in numerical simulations and in field observations [23].

As for other promising directions, the study of travelling waves in stratified flows [67, 68] is of great physical relevance, even if the complexities encountered here offer an even less transparent picture of what goes on beneath the waves. There are also some papers that investigate the setting of discontinuous vorticity distributions [18, 46]. For a more complete list of papers devoted to periodic travelling two-dimensional water waves with vorticity we refer to the discussion and the reference lists in [10, 29, 32, 47, 60].

We conclude our discussion by pointing out the fact that Stokes waves are modulationally unstable, a phenomenon also known as the Benjamin–Feir instability [3]: the uniform wave train loses energy to a small perturbation of other waves with nearly the same frequency and direction, thus disintegrating and forming complex three-dimensional wave patterns. The particle trajectories of such wave flows are not understood—see the recent discussion in [55].

Acknowledgments

Helpful comments and suggestions of the referee on an earlier draft of this paper and the support of the FWF Project I544-N13 ‘Lagrangian kinematics of water waves’ of the Austrian Science Fund are gratefully acknowledged.

References

[1] Amick C J 1987 Bounds for water waves *Arch. Ration. Mech. Anal.* **99** 91–114
[2] Amick C J, Fraenkel L E and Toland J F 1982 On the Stokes conjecture for the wave of extreme form *Acta Math.* **148** 193–214
[3] Benjamin T B and Feir J E 1967 The disintegration of wave trains on deep water *J. Fluid Mech.* **27** 417–30
[4] Bryson A E 1964 *Waves in Fluids (Film) (National Committee for Fluid Mechanics Films)* (Chicago, IL: Encyclopaedia Britannica Educational Corporation)
[5] Chen Y-Y, Hsu H-C and Chen G-Y 2010 Lagrangian experiment and solution for irrotational finite-amplitude progressive gravity waves at uniform depth *Fluid Dyn. Res.* **42** 045511
[6] Clamond D 2007 On the Lagrangian description of steady surface gravity waves *J. Fluid Mech.* **589** 433–54

[7] Clamond D 2012 Note on the velocity and related fields of steady irrotational two-dimensional surface gravity waves *Phil. Trans. R. Soc.* A **370** 1572–86
[8] Clamond D and Constantin A 2013 Recovery of steady periodic wave profiles from pressure measurements at the bed *J. Fluid Mech.* **714** 463–75
[9] Constantin A 2006 The trajectories of particles in Stokes waves *Inventiones Math.* **166** 523–35
[10] Constantin A 2011 Nonlinear water waves with applications to wave–current interactions and tsunamis *CBMS-NSF Conf. Series Application Mathematics* vol 81 (Philadelphia, PA: SIAM)
[11] Constantin A 2012 Particle trajectories in extreme Stokes waves *IMA J. Appl. Math.* **77** 293–307
[12] Constantin A 2013 Mean velocities in a Stokes wave *Arch. Ration. Mech. Anal.* **207** 907–17
[13] Constantin A 2014 Estimating wave heights from pressure data at the bed *J. Fluid Mech.* **743** R2
[14] Constantin A, Ehrnström M and Wahlén E 2007 Symmetry of steady periodic gravity water waves with vorticity *Duke Math. J.* **140** 591–603
[15] Constantin A and Escher J 2011 Analyticity of periodic traveling free surface water waves with vorticity *Ann. Math* **173** 559–68
[16] Constantin A and Strauss W 2004 Exact steady periodic water waves with vorticity *Commun. Pure Appl. Math.* **57** 481–527
[17] Constantin A and Strauss W 2010 Pressure beneath a Stokes wave *Commun. Pure Appl. Math.* **53** 533–57
[18] Constantin A and Strauss W 2011 Periodic traveling gravity water waves with discontinuous vorticity *Arch. Ration. Mech. Anal.* **202** 133–75
[19] Constantin A, Strauss W and Varvaruca E 2014 Global bifurcation of steady gravity water waves with critical layers arXiv:1407.0092
[20] Constantin A and Varvaruca E 2011 Steady periodic water waves with constant vorticity: regularity and local bifurcation *Arch. Ration. Mech. Anal.* **199** 33–67
[21] Constantin A and Villari G 2008 Particle trajectories in linear water waves *J. Math. Fluid Mech.* **10** 1–18
[22] Crapper G D 1984 *Introduction to Water Waves* (Chichester: Ellis Horwood)
[23] da Silva A F T and Peregrine D H 1988 Steep, steady surface waves on water of finite depth with constant vorticity *J. Fluid Mech.* **195** 281–302
[24] Debnath L 1994 *Nonlinear Water Waves* (Boston, MA: Academic)
[25] Dingemans D W 1997 *Water Wave Propagation Over Uneven Bottoms* (Singapore: World Scientific)
[26] Dubreil-Jacotin M-L 1934 Sur la détermination rigoureuse des ondes permanentes périodiques d'ampleur finie *J. Math. Pures Appl.* **13** 217–91
[27] Eames I and McIntyre M E 1999 On the connection between Stokes drift and Darwin drift *Math. Proc. Camb. Phil. Soc.* **126** 171–4
[28] Ehrnström M 2008 On streamlines and particle paths of gravitational water waves *Nonlinearity* **21** 1141–54
[29] Ehrnström M, Escher J and Wahlén E 2012 Steady water waves with multiple critical layers *J. Math. Fluid Mech.* **14** 407–19
[30] Fenton J D 1990 Nonlinear wave theories *The Sea* ed B LeMéhauté and D M Hanes (New York: Wiley-Interscience) pp 3–25
[31] Henry D 2009 Steady periodic flow induced by the Korteweg–de Vries equation *Wave Motion* **46** 403–11
[32] Henry D 2013 Large amplitude steady periodic waves for fixed-depth rotational flows *Commun. Partial Differ. Equ.* **38** 1015–37
[33] Ionescu-Kruse D 2008 Particle trajectories in linearized irrotational shallow water flows *J. Nonlinear Math. Phys.* **15** 13–27
[34] Johnson R S 1997 *A Modern Introduction to the Mathematical Theory of Water Waves* (Cambridge: Cambridge University Press)
[35] Jonsson I G 1990 Wave-current interactions *The Sea (Ocean Engineering Science* vol 9(A)) ed B Le Méhauté and D M Hanes (New York: Wiley) pp 65–120
[36] Kinsman B 1965 *Wind Waves* (Englewood Cliffs, NJ: Prentice-Hall)
[37] Ko J and Strauss W 2008 Effect of vorticity on steady water waves *J. Fluid Mech.* **608** 197–215
[38] Kogelbauer F 2015 Recovery of the wave profile for irrotational periodic water waves from pressure measurements *Nonlinear Anal. Real World Appl.* **22** 219–24
[39] Kozlov V and Kuznetsov N 2011 The Benjamin–Lighthill conjecture for steady water waves *Arch. Ration. Mech. Anal.* **201** 631–45

[40] Kozlov V and Kuznetsov N 2014 Dispersion equation for water waves with vorticity and Stokes Waves on flows with counter-currents *Arch. Ration. Mech. Anal.* **214** 971–1018
[41] Lighthill J 1978 *Waves in Fluids* (Cambridge: Cambridge University Press)
[42] Longuet-Higgins M S 1953 Mass transport in water waves *Phil. Trans. R. Soc.* A **245** 535–81
[43] Longuet-Higgins M S 1979 The trajectories of particles in steep, symmetric gravity waves *J. Fluid Mech.* **94** 497–517
[44] Longuet-Higgins M S 1983 On integrals and invariants for inviscid, irrotational flow under gravity *J. Fluid Mech.* **134** 155–9
[45] Longuet-Higgins M S 1986 Eulerian and Lagrangian aspects of surface waves *J. Fluid Mech.* **173** 683–707
[46] Martin C I and Matioc B-V 2014 Steady periodic water waves with unbounded vorticity: equivalent formulations and existence results *J. Nonlinear Sci.* **24** 633–59
[47] Matioc A-V and Matioc B-V 2013 On the symmetry of periodic gravity water waves with vorticity *Differ. Int. Equ.* **26** 129–40
[48] Milne-Thomson L M 1950 *Theoretical Hydrodynamics* (New York: The Macmillan Company)
[49] Nachbin A and Ribeiro-Junior R 2014 A boundary integral formulation for particle trajectories in Stokes waves *Discrete Continuous Dyn. Syst.* **34** 3135–53
[50] Okamoto H and Shoji M 2001 *The Mathematical Theory of Permanent Progressive Water Waves* (Singapore: World Scientific)
[51] Oliveras K L, Vasan V, Deconinck B and Henderson D 2012 Recovering the water-wave profile from pressure measurements *SIAM J. Appl. Math.* **72** 897–918
[52] Perlin M, Choi W and Tian Z 2013 Breaking waves in deep and intermediate waters *Annu. Rev. Fluid Mech.* **45** 115–45
[53] Plotnikov P I 1982 *Dinamika Sploshn. Sredy* **57** 41–76
Plotnikov P I 2002 Proof of the Stokes conjecture in the theory of surface waves *Stud. Appl. Math.* **108** 217–44 (Engl. transl.)
[54] Plotnikov P I and Toland J F 2004 Convexity of Stokes waves of extreme form *Arch. Ration. Mech. Anal.* **171** 349–416
[55] Punzmann H, Francois N, Xia H, Falkovich G and Shats M 2014 Generation and reversal of surface flows by propagating waves *Nat. Phys.* **10** 658–63
[56] Schwartz L W and Fenton J D 1982 Strongly nonlinear waves *Annu. Rev. Fluid Mech.* **14** 39–60
[57] Sommerfeld A 1950 *Mechanics of Deformable Bodies* (New York: Academic)
[58] Stoker J J 1957 *Water Waves: The Mathematical Theory with Applications* (New York: Interscience)
[59] Stokes G G 1880 *Mathematical and Physical Papers* (Cambridge: Cambridge University Press)
[60] Strauss W A 2010 Steady water waves *Bull. Am. Math. Soc.* **47** 671–94
[61] Struik D J 1926 Détermination rigoureuse des ondes irrotationelles périodiques dans un canal à profondeur finie *Math. Ann.* **95** 595–634
[62] Toland J F 1996 Stokes waves *Topological Methods Nonlinear Anal.* **7** 1–48
[63] Umeyama M 2012 Eulerian/Lagrangian analysis for particle velocities and trajectories in a pure wave motion using particle image velocimetry *Phil. Trans. R. Soc.* A **370** 1687–702
[64] Ursell F 1953 Mass transport in gravity waves *Proc. Camb. Phil. Soc.* **40** 145–50
[65] Varvaruca E 2008 Bernoulli free-boundary problems in strip-like domains and a property of permanent waves on water of finite depth *Proc. R. Soc. Edinburgh* A **138** 1345–62
[66] Wahlén E 2009 Steady water waves with a critical layer *J. Differ. Equ.* **246** 2468–83
[67] Walsh S 2009 Some criteria for the symmetry of stratified water waves *Wave Motion* **46** 350–62
[68] Walsh S, Bühler O and Shatah J 2013 Steady water waves in the presence of wind *SIAM J. Math. Anal.* **45** 2182–227
[69] Wang L J 2013 Regularity of traveling periodic stratified water waves with vorticity *Nonlinear Anal.* **81** 247–63